Revisiting pyramid compression to quantify flexoelectricity: a 3D simulation study

Amir Abdollahi, Daniel Millán, Christian Peco, Marino Arroyo, and Irene Arias*

Laboratori de Càlcul Numèric (LaCàN),

Universitat Politècnica de Catalunya (UPC),

Campus Nord UPC-C2, E-08034 Barcelona, Spain.†

(Dated: October 19, 2015)

Abstract

Flexoelectricity is a universal property of all dielectrics, by which they generate a voltage in response to an inhomogeneous deformation. One of the controversial issues in this field concerns the magnitude of flexoelectric coefficients measured experimentally, which greatly exceed theoretical estimates. Furthermore, there is a broad scatter amongst experimental measurements. The truncated pyramid compression method is one of the common setups to quantify flexoelectricity, the interpretation of which relies on simplified analytical equations to estimate strain gradients. However, the deformation fields in 3D pyramid configurations are highly complex, particularly around its edges. In the present work, using three-dimensional self-consistent simulations of flexoelectricity, we show that the simplified analytical estimations of strain gradients in compressed pyramids significantly overestimate flexoelectric coefficients, thus providing a possible explanation to reconcile different estimates. In fact, the interpretation of pyramid compression experiments is highly nontrivial. We systematically characterize the magnitude of this overestimation, of over one order of magnitude, as a function of the truncated pyramid configuration. These results are important to properly characterize flexoelectricity, and provide design guidelines for effective electromechanical transducers exploiting flexoelectricity.

PACS numbers: 77.65.-j, 77.80.bn, 77.90.+k

I. INTRODUCTION

Flexoelectricity is a two-way electromechanical coupling mechanism between electric polarization and strain gradients or strain and polarization gradients, rather than between polarization and strain as in piezoelectricity[1,2]. This material property may enable electromechanical transducers made out of non-piezoelectric materials[3–6], or new ways to address information in ferroelectric thin films[7]. Because strain gradients disrupt in general the inversion symmetry of the microscopic structure of a material, flexoelectricity is very general for dielectrics, unlike piezoelectricity, only present in non-centrosymmetric materials. On the other hand, flexoelectricity is strongly size-dependent because strain gradients are inversely proportional to structural size. Therefore, despite its universality, the flexoelectric effect is significant only at micro- and nanoscopic scales, making its experimental characterization challenging.

To quantitatively characterize flexoelectricity in different materials, measurements of direct flexoelectricity mechanically impose strain gradients in a sample and the induced voltage is recorded. Common setups to induce strain gradients in simple geometries include bending of thin films[8–10] and compression of truncated pyramids or cones[11,12]. It has been found that flexoelectric coefficients are particularly large in materials with high dielectric constants, such as ferroelectrics[9,11,13–15]. However, the magnitude of these coefficients greatly exceeds theoretical estimates[1,16,17]. This discrepancy has lead to a controversy in the field of flexoelectricity, demanding further investigations into the quantification of the flexoelectric response[18]. While recent developments in the field demonstrate that the surface contributions to the flexoelectric response may be a possible explanation[19–21], there is still a limited quantitative understanding on the flexoelectric coefficients. To translate an experimental measurement into a material parameter estimation, one must resort to a model. Here, we examine if the modeling assumptions underlying previous experimental estimations of flexoelectricity may provide a source of significant error.

The most widely used model for flexoelectricity is the linear continuum theory of flexoelectricity (see the recent reviews[18,22,23]). In this theory, flexoelectricity is represented by a fourth-order flexoelectric coupling tensor, whose symmetry is well understood[24–26]. Mathematically, the self-consistent electro-mechanical field equations of flexoelectricity are a coupled system of 4th order partial differential equations (PDEs). Despite analytical solu-

tions are starting to emerge for simple geometries and loads[27,28], most of the field operates with approximate solutions valid under very restrictive assumptions[11,29,30]. Furthermore, to interpret experiments, the two-way flexoelectric coupling is often ignored, by estimating strain gradients from elasticity alone[10].

To go beyond these simple approximate solutions, on can resort to computational methods, but because the equations involve high-order spatial derivatives, flexible methods such as conventional finite elements cannot be used. On rectangular or brick geometries, finite difference calculations have been applied to flexoelectricity[31–33]. To deal with more general geometries with non-uniform grid refinement, we have recently resorted to meshfree methods, relying on smooth basis functions[34], to solve numerically the continuum equations of flexoelectricity in 2D[35]. Surprisingly, we found that previous simplified calculations on beam and truncated triangle configurations provided only rough order-of-magnitude estimations of the flexoelectric response. These previous results suggest that in the 3D truncated pyramid configurations found in experiments, common simplified estimates may significantly deviate from the actual flexoelectric response. Our main objective in this paper is to revisit the pyramid compression method by performing realistic three-dimensional simulations of the self-consistent equations of linear flexoelectricity. In particular, we aim to evaluate the effect of pyramid geometry and boundary conditions on the flexoelectric response.

The structure of the paper is as follows. A summary of the continuum theory of flexoelectricity along with the computational model is presented in Section II. We then revisit the truncated pyramid experiment through 3D simulations in Section III and, in particular, discuss the sources of overestimation in the flexoelectric response. A systematic study of this response as a function of the truncated pyramid configuration are presented in Section IV. The last section is the conclusion.

II. THEORY, COMPUTATIONAL MODEL, AND MATERIAL PARAMETERS

The constitutive equation for the electric polarization $\mathbf{P}$ in a linear dielectric solid possessing flexoelectricity is[1]:

$$P_i = \chi_{ij} E_j + \mu_{klij} \nabla_j \varepsilon_{kl}, \tag{1}$$

where $\mathbf{E}$ is the electric field and ε is the mechanical strain. The dielectric response is described by the first term, where χ is the second-order dielectric susceptibility tensor. The

flexoelectric effect is introduced by the second term, where μ is the fourth-order tensor of flexoelectricity and $\nabla\varepsilon$ is the strain gradient. Given the electric polarization in Eq. (1), the electric displacement $\mathbf{D}$ is obtained as

$$D_i = \varepsilon_0 E_i + P_i = \kappa_{ij} E_j + \mu_{klij} \nabla_j \varepsilon_{kl}, \tag{2}$$

where ε_0 is the permittivity of free space and κ_{ij} is the second-order dielectric tensor. Equation (2) determines the electrostatic state of the solid, where the electric field derives from the electric potential ϕ, $E_i = -\phi_{,i}$.

The thermodynamically conjugated effect to the direct flexoelectric response in Eq. (2) is the *converse flexoelectric effect*, introduced via the constitutive equation for the mechanical stress σ

$$\sigma_{ij} = \mathbb{C}_{ijkl}\varepsilon_{kl} + \mu_{lijk} E_{l,k} - h_{ijklmn}\varepsilon_{lm,nk}, \tag{3}$$

where the first term is the elastic response, $\mathbb{C}$ being the fourth-order tensor of elastic moduli. The converse flexoelectric effect is through the third term, where $\nabla\mathbf{E}$ is the electric field gradient. The last term is the strain-gradient elastic response, $\mathbf{h}$ being the sixth-order strain-gradient elasticity tensor. This term guarantees the well-posedness of the flexoelectric equations[28,36–38].

Equations (2) and (3) can be shown to derive from an electro-mechanical enthalpy energy density for the linear flexoelectric solid

$$\begin{aligned}\mathcal{H}(\varepsilon_{ij}, E_i, \varepsilon_{jk,l}) = \tfrac{1}{2}\mathbb{C}_{ijkl}\varepsilon_{ij}\varepsilon_{kl} - \mu_{ijkl}E_i\varepsilon_{jk,l} - \tfrac{1}{2}\kappa_{ij}E_iE_j \\ + \tfrac{1}{2}h_{ijklmn}\varepsilon_{ij,k}\varepsilon_{lm,n},\end{aligned} \tag{4}$$

as

$$\hat{\sigma}_{ij} = \frac{\partial \mathcal{H}}{\partial \varepsilon_{ij}}, \quad \widetilde{\sigma}_{ijk} = \frac{\partial \mathcal{H}}{\partial \varepsilon_{ij,k}}, \quad \hat{D}_i = -\frac{\partial \mathcal{H}}{\partial E_i}, \tag{5}$$

where the mechanical stress is obtained from the usual contribution $\hat{\sigma}$ and the higher-order (hyper) stress $\widetilde{\sigma}$ as

$$\sigma_{ij} = \hat{\sigma}_{ij} - \widetilde{\sigma}_{ijk,k}. \tag{6}$$

The total enthalpy of the system results from integrating $\mathcal{H}$ over the domain, and accounting for the contributions of the external loadings. We refer to Ref.[35] for a complete description of the theory and its Galerkin numerical discretization. For the reader's convenience, we provide in A details about the numerical implementation in 3D. We have carefully checked numerical convergence, as shown in Fig. 2.

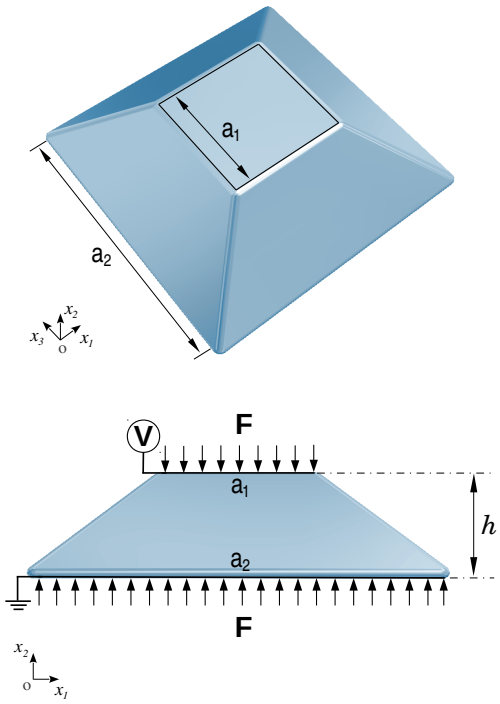

FIG. 1. Truncated pyramid under the mechanical load F, uniformly distributed at the top and bottom surfaces. The top square face has length a_1 and the bottom length a_2. The electric potential is fixed to zero at the bottom and is constant but unknown at the top. The edges of the geometry have been rounded to avoid unphysical singularities.

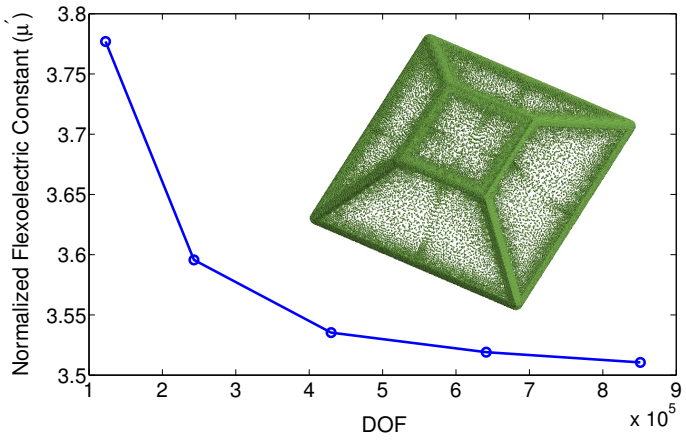

FIG. 2. Convergence study of the numerical simulations. Normalized flexoelectric constant μ' as a function of the number of degrees of freedom (DOF), i.e. the number of nodes times 4 (3 components of the displacement field and the electric potential). The inset shows a representative computational node set.

To perform numerical simulations, we consider truncated pyramid geometries as shown in Fig. 1. A total force of magnitude F is applied uniformly at the top and bottom square faces, whose lateral dimensions are a_1 and a_2. The electric potential is fixed to zero at the bottom and to a constant but *a priori* unknown value V at the bottom electrode, which is found as a result of the numerical calculation.

The material constants are chosen to fit the behavior of a strongly flexoelectric material, Barium Strontium Titanate (BST) in its non-piezoelectric (paraelectric) phase at room temperature. We adopt a simple choice for the symmetry of the material tensors, but general enough to capture the multi-dimensional couplings of the field equations. We consider isotropic elasticity and permittivity and adopt cubic symmetry for the flexoelectric tensor. Therefore, there are only two independent elastic constants, the Young's modulus E and the Poisson's ratio ν, one dielectric permittivity constant κ_{11}, two strain-gradient elasticity constants h_{111111} and h_{122122} (or in matrix notation h_{11} and h_{12}, see A), and three independent flexoelectric coefficients, μ_{1111}, μ_{1221}, and μ_{1212} (or in matrix notation μ_{11}, μ_{12}, and μ_{44}). Here, we only consider the longitudinal and transversal flexoelectric coefficients, μ_{11} and μ_{12}, since the shear coefficient μ_{44} is poorly characterized. All the material tensors and parameters are described in A.

III. REVISITING THE TRUNCATED PYRAMID EXPERIMENT THROUGH 3D SIMULATIONS

The applied force on the truncated pyramid generates different tractions at the top and bottom surfaces due to their different areas. As a result, a strain gradient and thus a flexoelectric polarization are generated. Thus, but adopting a pyramid geometry, a non-piezoelectric solid behaves effectively as a piezoelectric solid. To quantify this effective piezoelectricity, one can consider a comparison piezoelectric solid with a parallelepiped geometry of square base of size a_2, height h, and piezoelectric coupling tensor $\mathbf{e}$, which produces the same polarization as the flexoelectric solid with pyramid geometry. Let us assume that the material only has non-zero longitudinal flexoelectric coefficient μ_{11} and elastic constant $c_{11} = E(1-\nu)/(1+\nu)(1-2\nu)$, and that the through-thickness longitudinal strain ε_{22} is the only non-zero component. In the piezoelectric solid, strain is constant and given by $\bar{\varepsilon}_{22} = F/(c_{11}a_2^2)$. In the pyramid, by interpolating linearly the strain at top and bottom

surfaces, the strain gradient can be estimated as $\varepsilon_{22,2} = \bar{\varepsilon}_{22}(R-1)/h$, where $R = (a_2/a_1)^2$ is the area ratio, see Fig. 1. Then, the equation equating the polarization in the flexoelectric pyramid and in the comparison piezoelectric solid

$$e_{ijk}\varepsilon_{jk} = \mu_{klij}\nabla_j\varepsilon_{kl}, \tag{7}$$

simplifies to[11],

$$e_{33} = \mu_{11}\left(\frac{R-1}{h}\right), \tag{8}$$

providing a definition for the effective piezoelectric constant e_{33} of the pyramid. Experimentally, if the electric potential difference between electrodes V resulting from an applied force F is recorded, e_{33} can also be computed by dividing the nominal polarization in the sample $-\chi_{11}V/h$ by the nominal strain as

$$e_{33} = -\frac{\chi_{11}V}{h\bar{\varepsilon}_{22}}. \tag{9}$$

Combining Eqs. (9) and (8), the flexoelectric constant μ_{11} of the material can be estimated as

$$\mu_{11}^{\text{est}} = -\frac{\chi_{11}V}{(R-1)\bar{\varepsilon}_{22}}. \tag{10}$$

By performing an electromechanically self-consistent 3D simulation of the experiment, it is also possible to estimate the flexoelectric coefficient using Eq. (10). The difference now is that the actual flexoelectric coefficient μ_{11} used to produce the simulation is known, and therefore we can define a normalized flexoelectric constant $\mu' = \mu_{11}^{\text{est}}/\mu_{11}$, measuring the accuracy of the simple estimation used to interpret experiments. If the analytical formula in (10) is a good estimate of the flexoelectric response, the normalized flexoelectric constant μ' should be close to one.

To examine this point, we perform a case study simulation inspired in the work of Ref.[3], where experiments were performed on an array of truncated pyramids under compression. In these experiments, electrodes were deposited on the top and bottom sides of the pyramids to collect the induced charges. The dimensions of the pyramids in the experiments, also used here, are $a_2 = 2.72$ mm, $a_1 = 1.13$ mm, and h=0.76 mm. The 3-D simulation of this pyramid, subjected to a load of F=200 N, predict an induced voltage of V = -17.1 V on the top electrode, as shown in Fig. 3(a). With these data, a normalized flexoelectric constant $\mu' = 3.5$ is obtained, indicating more than a three-fold overestimation of the flexoelectric constant by the simple analytical estimate.

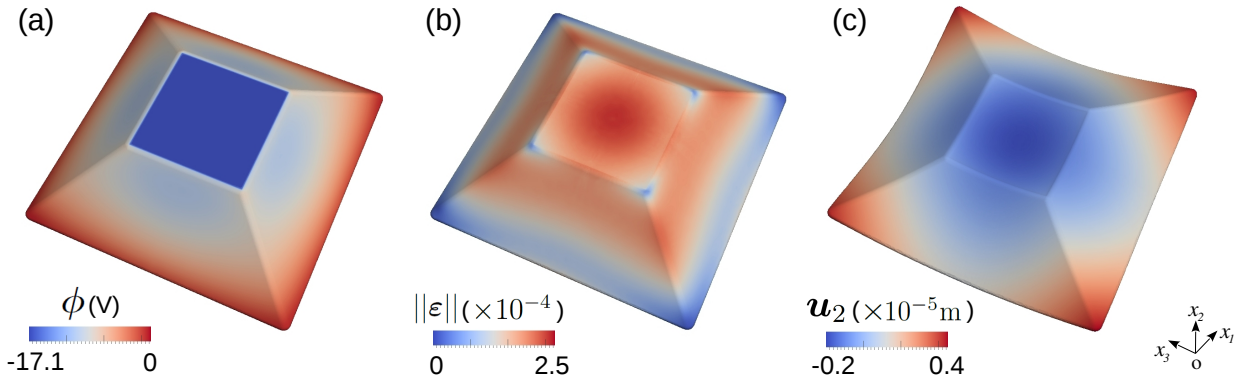

FIG. 3. Distribution of (a) the electric potential ϕ and (b) the strain norm $||\varepsilon||$ in the truncated pyramid under compression. (c) Distribution of the through-thickness mechanical displacement u_2 in the deformed configuration of the pyramid. The deformation is exaggerated by a factor of 10 for clarity.

To understand the origin of the overestimation, we plot the distribution of the strain norm $||\varepsilon|| := (\varepsilon : \varepsilon)^{1/2}$ in Fig. 3(b) together with the distribution of the through-thickness mechanical displacement u_2 in the deformed configuration of the pyramid in Fig. 3(c). Sharp changes of the strain are observed, particularly near the pyramid corners in Fig. 3(b), resulting in a significant and localized flexoelectric effect. This is in contrast to the assumptions underlying the analytical estimates, where a 1-D homogeneous distribution of the strain gradient is assumed. Furthermore, Fig. 3(c) shows that the pyramid undergoes a bending deformation in addition to the compressive deformation. Therefore, another important source of discrepancy is the bending deformation mode of the pyramid, mobilizing the transversal flexoelectric components neglected in the analytical model. In this simulation, a fully flexible support of the pyramid is considered, which uniformly distributes tractions as shown in Fig. 1. We consider later rigidly supported pyramids. Thus, both strain gradient localization due to compression and bending-induced strain gradients result in a higher effective flexoelectric response as compared to the naive calculation, resulting in an overestimation of the flexoelectric coefficient.

IV. SYSTEMATIC DEPENDENCE OF EFFECTIVE FLEXOELECTRIC COEFFICIENT ON GEOMETRY AND BOUNDARY CONDITIONS

These results suggest that simple estimations such as those leading to Eq. (10) are not reliable to compute the flexoelectric response of truncated pyramids. In principle, the overestimation indicated by the normalized flexoelectric constant μ' should strongly depend on the configuration and boundary conditions of the pyramid. To support this hypothesis, we perform a set of simulations considering different area ratios (R) and inclination angles (α) of the truncated pyramid. Figure 4 presents the results for different pyramid configurations. It is clear that the overestimation increases noticeably by decreasing the area ratio and/or the inclination angle of the pyramid. The deformation (inset) shows that the main source of the overestimation is the bending deformation of the pyramid. For high inclination angle and high area ratio pyramids, the response is dominated by the compressive deformation mode and the normalized flexoelectric constant approaches unity, i.e. the overestimation decreases. On the other hand, for low inclination angles and low area ratios, the pyramid approaches a plate configuration and the response is mainly due to the bending deformation mode. In this situation, the assumption of pure compressive deformation in Eq. (8) is not valid, leading to a noticeable overestimation of the flexoelectric constant (up to $\mu' = 45$ for $R = 2.2$ and $\alpha = 20^o$). This may partially explain the discrepancy between experimental measurements using the pyramid compression method and theoretical estimates[18].

The flexoelectric response of truncated pyramids also strongly depends on boundary conditions. To highlight this point, we perform additional simulations of the truncated pyramid by assuming a rigid bottom support, which constraints the displacements of the bottom face of the pyramid. In this situation, a non-uniform traction is induced on the bottom surface. We consider only the pyramids with an inclination angle of $\alpha = 45^o$, which are the most common configurations[11]. The results in Fig. 4 show that the overestimation of the flexoelectric constant decreases for rigidly supported pyramids, where the bending deformation are precluded. However, we still observe an overestimation of the flexoelectric constant due to sharp changes of the strain field near the pyramid corners, as discussed earlier in Fig. 3(b). For intermediate conditions, where the bottom support is not fully rigid nor flexible, μ' lies between the rigid and flexible results. By way of example, for the pyramid building unit in the experiments of Ref.[3], we obtain $\mu' = 3.5$ in the flexibly

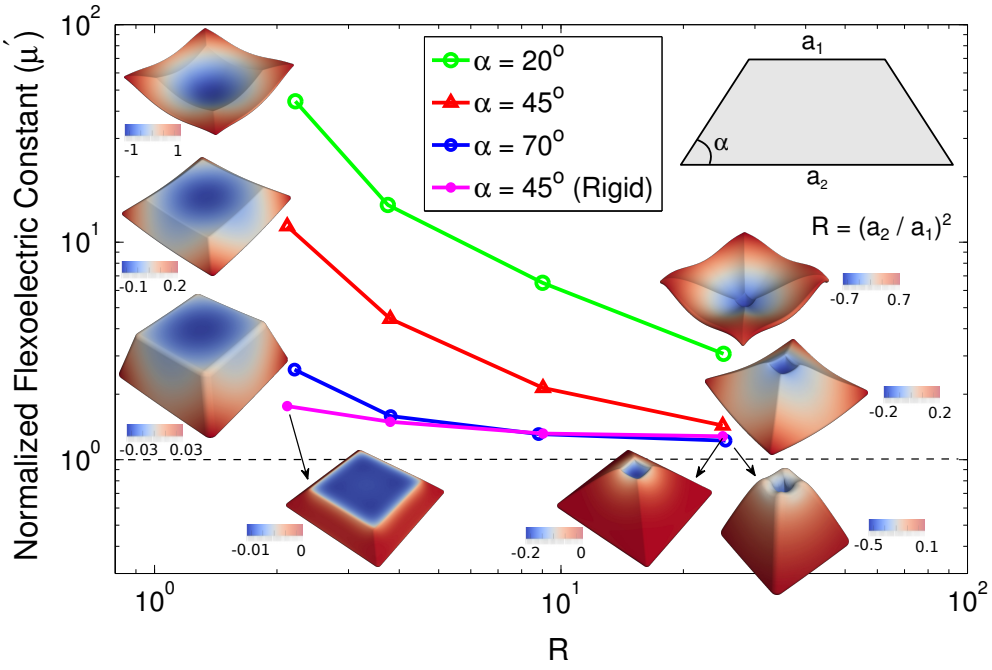

FIG. 4. Normalized flexoelectric constant μ' as a function of the pyramid area ratio R. The results are obtained considering different inclination angles α. The inset shows the distribution of the through-thickness displacement (u_2) in the deformed configuration of the pyramid for the lowest and highest area ratios. The deformation is exaggerated by a factor of 10 for clarity. The color bar indicates the displacement scale in each case, normalized by a factor of 10^{-5}m.

supported case and $\mu' = 1.3$ in the rigidly supported case. Since in these experiments the pyramid building unit is mounted on a semi-rigid BST ceramic sheet, we expect an intermediate overestimation.

The results in Fig. 4 for a flexible support can be summarized by the following fit

$$\ln \mu' \approx 7.1 - 2.6 \ln R - 5.2\alpha + 0.30 (\ln R)^2 + 0.88\alpha \ln R + 0.85\alpha^2, \tag{11}$$

where α is expressed in radians. This equation provides a simple way to correct the simplified estimate in Eq. (10) for pyramids on a flexible support, which should be divided by μ'. For a rigid support, the overestimation is weakly dependent on R (for $\alpha = 45°$, it ranges from 1.3 to 1.6). Thus, our results show that the pyramid compression test is complex to interpret, particularly when the support is flexible. The simple estimate in Eq. (10) provides a reasonable approximation when the support is much more rigid than the flexoelectric sample.

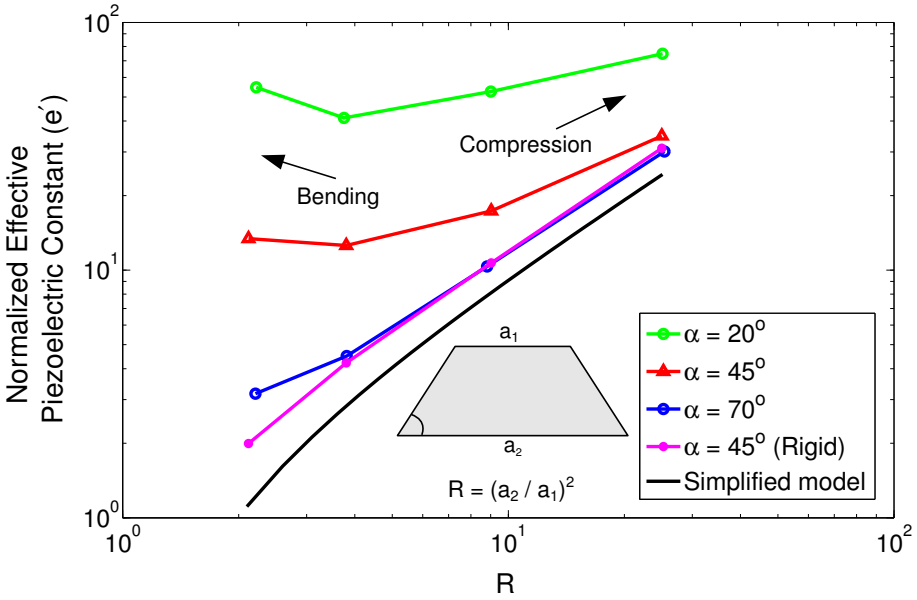

FIG. 5. Normalized effective piezoelectric constant e' as a function of the pyramid area ratio R. The results are obtained considering different values of the inclination angle α. The result of the simplified analytical model, $e' = R - 1$, is also plotted for comparison purposes.

The simulations can also be used to design electromechanical transducers based on flexoelectric truncated pyramids, which exhibit high effective piezoelectric effect thanks to a careful geometric configuration. For this purpose, we define the normalized effective piezoelectric constant $e' = he_{33}/\mu_{11}$ as a design criterion, where e_{33} is obtained in Eq. (9) using the simulation results. This coefficient measures the efficiency with which the flexoelectricity is exploited to obtain an effective piezoelectricity. Figure 5 presents this constant for different pyramid configurations. For comparison purposes, the result of the simplified analytical model in Eq. (8), $e' = R - 1$, is also plotted. For high area ratio pyramids where the compressive deformation is dominant, the effective response follows quite closely the analytical estimation. However, by decreasing this ratio, the bending deformation becomes more prominent, overweighting the decreasing effect of the compressive mode. This enhancing effect due to bending is more noticeable for lower inclination angles. The role of the bending deformation becomes evident by comparing the response of the flexible and rigid support pyramids ($\alpha = 45^o$) in Fig. 5. As expected, in the absence of the bending deformation in the rigidly support configuration, the response closely follows the simplified analytical model. In contrast, if allowed to bend by the flexible support, the system becomes a much more

efficient flexoelectric transducer, increasing the effective electromechanical coupling by an order of magnitude for small area ratios.

As discussed earlier, the bending deformation dominates the response in pyramids with low inclination angles and low area ratios, e.g. $\alpha = 20^o$ and $R = 2.2$. In this regime, the pyramid shape is similar to a plate configuration. By further decreasing the area ratio, the plate thickness decreases as well, magnifying the transversal strain gradient due to bending. This effect explains the flexoelectric response enhancement observed in pyramids with $\alpha = 20^o$ and $\alpha = 45^o$ below a certain area ratio. In general, the lower is the inclination angle of the pyramid, the higher is the effective electromechanical coupling. In summary, configurations generating strain gradients as a result of compressive stresses distributed over a non-uniform cross-section are not as efficient flexoelectric electromechanical transducers as configurations introducing strain gradients though bending (pyramids of small angle α). However, pyramidal systems mobilizing bending develop complex strain gradient states, and therefore they may be inadequate for material characterization. High area-ratio (R) pyramids of intermediate or high angle α may strike a compromise since they exhibit significant flexoelectric transduction, their response is weakly dependent on boundary conditions and angle, and they may be reasonably approximated using the simplified model underlying Eq. (10), which only overestimates the flexoelectric coefficient by a few-fold.

V. CONCLUSIONS

We have performed, to the best of our knowledge, the first 3-D simulations of linear flexoelectricity in dielectric solids. The simulations are based on a continuum model of flexoelectricity, in which the resulting high-order coupled partial differential equations are numerically approximated using meshfree approximants and a Galerkin method. We have revisited the pyramid compression method, which is one of the common setups for quantifying the flexoelectric response. This configuration is computationally challenging since the complex fields near the pyramid edges need to be resolved accurately. The simulation results show that a simple analytical estimates used to interpret truncated pyramid experiments overestimate the flexoelectric constant. This observation can partially explain the discrepancy between different experimental measurements and theoretical estimates[18]. We have found that the sources of the overestimation are (1) strain gradients localized around geo-

metric features, and (2) bending deformations when pyramids lie on a flexible support, and that these effects strongly depend on geometry and boundary conditions. Suppressing these sources of additional strain gradients minimize the overestimation, and therefore render the simplified estimations accurate. However, exacerbating additional strain gradients, either by considering low area ratio configurations or by reducing the pyramid inclination angle α on flexible supports, can significantly increase the effective electromechanical coupling of the device induced by flexoelectricity.

ACKNOWLEDGEMENTS

The authors gratefully acknowledge the support of the Ministerio de Ciencia e Innovación (DPI2011-26589), and the computer resources, technical expertise and assistance provided by the Barcelona Supercomputing Center - Centro Nacional de Supercomputación.

Appendix A: Numerical approximation and convergence analysis

Meshfree methods provide an approximation to continuum field equations based on basis functions that do not rely on a mesh or its connectivity. In recent years, the information theoretic concept of maximum-entropy has been put forth to develop meshfree approximation schemes, in particular the local maximum-entropy (LME) approximants[34,39]. Essentially, these methods allows us to determine a set of smooth basis functions $p^a(\mathbf{x})$, each localized around its corresponding node of the grid. We expand the continuum displacement and electric potential fields as

$$\mathbf{u}(\mathbf{x}) = \sum_{a=1}^{N} p^a(\mathbf{x})\mathbf{u}^a, \qquad \phi(\mathbf{x}) = \sum_{a=1}^{N} p^a(\mathbf{x})\phi^a,$$

and their derivatives as

$$\begin{aligned}
\partial_j u_i &= \textstyle\sum_{a=1}^{N} \partial_j p^a u_i^a, \\
\partial_j \partial_k u_i &= \textstyle\sum_{a=1}^{N} \partial_j \partial_k p^a u_i^a, \\
\partial_j \phi &= \textstyle\sum_{a=1}^{N} \partial_j p^a \phi^a,
\end{aligned}$$

where the first and second variations involve the gradient and Hessian of the LME basis functions, respectively. From now on, we omit the arguments of the basis functions for simplicity, i.e. $\mathbf{u} = \sum_{a=1}^{N} p^a \mathbf{u}^a$.

Introducing these expansions into the continuum total electromechanical enthalpy[35], we obtain its discrete representation as

$$\begin{aligned}
H(\mathbf{U},\phi) = &\frac{1}{2}\sum_{a,b} \mathbf{u}^{aT} \left(\int_\Omega \mathbf{B}_\mathbf{u}(p^a) \mathbb{C} \mathbf{B}_\mathbf{u}{}^T(p^b) d\Omega \right) \mathbf{u}^a \\
&+ \sum_{a,b} \mathbf{u}^{aT} \left(\int_\Omega \mathbf{H}_\mathbf{u}(p^a) \mu^T \mathbf{B}_\phi^T(p^b) d\Omega \right) \phi^b \\
&- \frac{1}{2}\sum_{a,b} \left(\int_\Omega \mathbf{B}_\phi(p^a) \mathbf{K} \mathbf{B}_\phi^T(p^b) d\Omega \right) \phi^a \phi^b \\
&+ \frac{1}{2}\sum_{a,b} \mathbf{u}^{aT} \left(\int_\Omega \mathbf{H}_\mathbf{s}(p^a) \mathbf{h} \mathbf{H}_\mathbf{s}{}^T(p^b) d\Omega \right) \mathbf{u}^a \\
&- \sum_a \left(\int_{\Gamma_t} \bar{\mathbf{t}} p^a \, \mathrm{d}S \right) \mathbf{u}^a + \sum_a \left(\int_{\Gamma_D} \omega p^a \, \mathrm{d}S \right) \phi^a,
\end{aligned}$$

$\bar{\mathbf{t}}$ are the imposed mechanical tractions, and ω the prescribed change density. The stiffness tensor $\mathbb{C}$, the dielectric tensor $\mathbf{K}$, the flexoelectric tensor μ, and the strain-gradient tensor

h have been written in Voigt form as

$$\mathbb{C} = \begin{bmatrix} c_{11} & c_{12} & c_{12} & 0 & 0 & 0 \\ c_{12} & c_{11} & c_{12} & 0 & 0 & 0 \\ c_{12} & c_{12} & c_{11} & 0 & 0 & 0 \\ 0 & 0 & 0 & c_{44} & 0 & 0 \\ 0 & 0 & 0 & 0 & c_{44} & 0 \\ 0 & 0 & 0 & 0 & 0 & c_{44} \end{bmatrix},$$

$$\mathbf{K} = \begin{bmatrix} \kappa_{11} & 0 & 0 \\ 0 & \kappa_{11} & 0 \\ 0 & 0 & \kappa_{11} \end{bmatrix},$$

$$\mu = \begin{bmatrix} \mu_{11} & 0 & 0 & \mu_{12} & 0 & 0 & \mu_{12} & 0 & 0 & 0 & \mu_{44} & 0 & 0 & 0 & \mu_{44} & 0 & 0 & 0 \\ 0 & \mu_{12} & 0 & 0 & \mu_{11} & 0 & 0 & \mu_{12} & 0 & \mu_{44} & 0 & 0 & 0 & 0 & 0 & 0 & 0 & \mu_{44} \\ 0 & 0 & \mu_{12} & 0 & 0 & \mu_{12} & 0 & 0 & \mu_{11} & 0 & 0 & 0 & \mu_{44} & 0 & 0 & 0 & \mu_{44} & 0 \end{bmatrix},$$

$$\mathbf{h} = l_1^2 \begin{bmatrix}
c_{11} & 0 & 0 & 0 & c_{12} & c_{12} & 0 & 0 & 0 & 0 & 0 & 0 & 0 & 0 & 0 & 0 & 0 \\
0 & c_{11} & 0 & c_{12} & 0 & 0 & 0 & 0 & c_{12} & 0 & 0 & 0 & 0 & 0 & 0 & 0 & 0 \\
0 & 0 & c_{11} & 0 & 0 & 0 & c_{12} & c_{12} & 0 & 0 & 0 & 0 & 0 & 0 & 0 & 0 & 0 \\
0 & c_{12} & 0 & c_{11} & 0 & 0 & 0 & 0 & c_{12} & 0 & 0 & 0 & 0 & 0 & 0 & 0 & 0 \\
c_{12} & 0 & 0 & 0 & c_{11} & c_{12} & 0 & 0 & 0 & 0 & 0 & 0 & 0 & 0 & 0 & 0 & 0 \\
c_{12} & 0 & 0 & 0 & c_{12} & c_{11} & 0 & 0 & 0 & 0 & 0 & 0 & 0 & 0 & 0 & 0 & 0 \\
0 & 0 & c_{12} & 0 & 0 & 0 & c_{11} & c_{12} & 0 & 0 & 0 & 0 & 0 & 0 & 0 & 0 & 0 \\
0 & 0 & c_{12} & 0 & 0 & 0 & c_{12} & c_{11} & 0 & 0 & 0 & 0 & 0 & 0 & 0 & 0 & 0 \\
0 & c_{12} & 0 & c_{12} & 0 & 0 & 0 & 0 & c_{11} & 0 & 0 & 0 & 0 & 0 & 0 & 0 & 0 \\
0 & 0 & 0 & 0 & 0 & 0 & 0 & 0 & 0 & c_{44} & 0 & 0 & 0 & 0 & 0 & 0 & 0 \\
0 & 0 & 0 & 0 & 0 & 0 & 0 & 0 & 0 & 0 & c_{44} & 0 & 0 & 0 & 0 & 0 & 0 \\
0 & 0 & 0 & 0 & 0 & 0 & 0 & 0 & 0 & 0 & 0 & c_{44} & 0 & 0 & 0 & 0 & 0 \\
0 & 0 & 0 & 0 & 0 & 0 & 0 & 0 & 0 & 0 & 0 & 0 & c_{44} & 0 & 0 & 0 & 0 \\
0 & 0 & 0 & 0 & 0 & 0 & 0 & 0 & 0 & 0 & 0 & 0 & 0 & c_{44} & 0 & 0 & 0 \\
0 & 0 & 0 & 0 & 0 & 0 & 0 & 0 & 0 & 0 & 0 & 0 & 0 & 0 & c_{44} & 0 & 0 \\
0 & 0 & 0 & 0 & 0 & 0 & 0 & 0 & 0 & 0 & 0 & 0 & 0 & 0 & 0 & c_{44} & 0 \\
0 & 0 & 0 & 0 & 0 & 0 & 0 & 0 & 0 & 0 & 0 & 0 & 0 & 0 & 0 & 0 & c_{44}
\end{bmatrix}, \tag{}$$

where $c_{11} = E(1-\nu)/(1+\nu)(1-2\nu)$, $c_{12} = E\nu/(1+\nu)(1-2\nu)$, and $c_{44} = (c_{11} - c_{12})/2$. The value of μ_{12} is chosen to be equal to μ_{11} and it is assumed that $\mu_{44} = 0$. With these parameters and following[28], we obtain a conservative value for the length scale l_1, to guarantee positive definiteness of the strain energy. The material parameters of BST[3,40] are presented in Table I.

TABLE I. Material parameters

E	ν	μ_{11}	κ_{11}	l_1
152 GPa	0.33	121 μC/m	141.6 nC/Vm	10 nm

The gradient operators $\mathbf{B_u}$ and $\mathbf{B}_\phi$ and the Hessian operators $\mathbf{H_u}$ and $\mathbf{H_s}$ can be written

in Voigt form as

$$\mathbf{B_u} = \begin{bmatrix} \partial/\partial x & 0 & 0 & \partial/\partial y & 0 & \partial/\partial z \\ 0 & \partial/\partial y & 0 & \partial/\partial x & \partial/\partial z & 0 \\ 0 & 0 & \partial/\partial z & 0 & \partial/\partial y & \partial/\partial x \end{bmatrix},$$

$$\mathbf{B}_\phi = \begin{bmatrix} \partial/\partial x & \partial/\partial y & \partial/\partial z \end{bmatrix},$$

$$\mathbf{H_u} = \begin{bmatrix} \frac{\partial^2}{\partial x^2} & \frac{\partial^2}{\partial x \partial y} & \frac{\partial^2}{\partial x \partial z} & 0 & 0 & 0 & 0 & 0 & 0 \\ 0 & 0 & 0 & \frac{\partial^2}{\partial y \partial x} & \frac{\partial^2}{\partial y^2} & \frac{\partial^2}{\partial y \partial z} & 0 & 0 & 0 \\ 0 & 0 & 0 & 0 & 0 & 0 & \frac{\partial^2}{\partial z \partial x} & \frac{\partial^2}{\partial z \partial y} & \frac{\partial^2}{\partial z^2} \end{bmatrix} \dots$$

$$\dots \begin{bmatrix} \frac{\partial^2}{\partial y \partial x} & \frac{\partial^2}{\partial y^2} & \frac{\partial^2}{\partial y \partial z} & \frac{\partial^2}{\partial z \partial x} & \frac{\partial^2}{\partial z \partial y} & \frac{\partial^2}{\partial z^2} & 0 & 0 & 0 \\ \frac{\partial^2}{\partial x^2} & \frac{\partial^2}{\partial x \partial y} & \frac{\partial^2}{\partial x \partial z} & 0 & 0 & 0 & \frac{\partial^2}{\partial z \partial x} & \frac{\partial^2}{\partial z \partial y} & \frac{\partial^2}{\partial z^2} \\ 0 & 0 & 0 & \frac{\partial^2}{\partial x^2} & \frac{\partial^2}{\partial x \partial y} & \frac{\partial^2}{\partial x \partial z} & \frac{\partial^2}{\partial y \partial x} & \frac{\partial^2}{\partial y^2} & \frac{\partial^2}{\partial y \partial z} \end{bmatrix},$$

$$\mathbf{H_s} = \begin{bmatrix} \frac{\partial^2}{\partial x^2} & 0 & 0 & \frac{\partial^2}{\partial x \partial y} & 0 & 0 & \frac{\partial^2}{\partial x \partial z} & 0 & 0 \\ 0 & \frac{\partial^2}{\partial y^2} & 0 & 0 & \frac{\partial^2}{\partial y \partial x} & 0 & 0 & \frac{\partial^2}{\partial y \partial z} & 0 \\ 0 & 0 & \frac{\partial^2}{\partial z^2} & 0 & 0 & \frac{\partial^2}{\partial z \partial x} & 0 & 0 & \frac{\partial^2}{\partial z \partial y} \end{bmatrix} \dots$$

$$\dots \begin{bmatrix} \frac{\partial^2}{\partial y \partial x} & \frac{\partial^2}{\partial z \partial x} & 0 & \frac{\partial^2}{\partial y^2} & \frac{\partial^2}{\partial z \partial y} & \frac{\partial^2}{\partial y \partial z} & \frac{\partial^2}{\partial z^2} & \frac{\partial^2}{\partial y \partial z} & 0 \\ \frac{\partial^2}{\partial x^2} & 0 & \frac{\partial^2}{\partial z \partial x} & \frac{\partial^2}{\partial x \partial y} & 0 & \frac{\partial^2}{\partial x \partial z} & 0 & \frac{\partial^2}{\partial x \partial z} & \frac{\partial^2}{\partial z^2} \\ 0 & \frac{\partial^2}{\partial x^2} & \frac{\partial^2}{\partial y \partial x} & 0 & \frac{\partial^2}{\partial x \partial y} & 0 & \frac{\partial^2}{\partial x \partial z} & 0 & \frac{\partial^2}{\partial y \partial z} \end{bmatrix}.$$

The discrete algebraic equations for the equilibrium can be derived following the usual Galerkin procedure as

$$\begin{bmatrix} \mathbf{A_{UU}} & \mathbf{A}_{\mathbf{U}\phi} \\ \mathbf{A}_{\phi\mathbf{U}} & \mathbf{A}_{\phi\phi} \end{bmatrix} \begin{bmatrix} \mathbf{U} \\ \phi \end{bmatrix} = \begin{bmatrix} \mathbf{f_U} \\ \mathbf{f}_\phi \end{bmatrix},$$

where the local contribution of each quadrature point to the matrix of system has the structure

$$\mathbf{A}^{ab}_{\mathbf{UU}} = \mathbf{B_u}(p^a)\mathbb{C}\mathbf{B_u}^T(p^b) + \mathbf{H_s}(p^a)\mathbf{h}\mathbf{H_s}^T(p^b),$$

$$\mathbf{A}^{ab}_{\mathbf{U}\phi} = \mathbf{H_u}(p^a)\mu^T\mathbf{B}^T_\phi(p^b),$$

$$\mathbf{A}^{ab}_{\phi\mathbf{U}} = \mathbf{B}_{\phi}(p^b)\mu{\mathbf{H}_{\mathbf{u}}}^T(p^a),$$

$$\mathbf{A}^{ab}_{\phi\phi} = -\mathbf{B}_{\phi}(p^a)\mathbf{K}\mathbf{B}^T_{\phi}(p^b),$$

$$\mathbf{f}_{\mathbf{U}} = \overline{\mathbf{t}}p^a, \mathbf{f}_{\phi} = -\omega p^a,$$

where the derivatives of the basis functions are evaluated at the corresponding quadrature point.

To assure the accuracy of the results, we perform a convergence analysis through a number of simulations. The pyramid configuration presented in Section III is chosen for the analysis and is discretized with five node sets of variable resolution. To capture the sharp changes of the strain and electric field near the edges of the pyramid, the nodal spacing is chosen to be smaller near the edges than in the bulk. To increase the resolution of each node set, the nodal spacing is decreased near the pyramid edges. Figure 2 presents the normalized flexoelectric constant μ' as a function of the number of degrees of freedom (DOF). The convergence of the results is clear from Fig. 2. The convergence is slow since a fine node distribution is required to properly capture the localized effects at the pyramid edges. In all simulations, we build a Delaunay tetrahedralization of each node set and generate a standard Gauss-Legendre quadrature rule of 11 points per tetrahedron, an overkill integration rule.

---

* irene.arias@upc.edu

† http://www.lacan.upc.edu

[1] S. M. Kogan, Sov. Phys. Solid State **5**, 2069 (1964).

[2] A. K. Tagantsev, Phys. Rev. B **34**, 5883 (1986).

[3] W. Zhu, J. Y. Fu, N. Li, and L. Cross, Appl. Phys. Lett. **89**, 192904 (2006).

[4] B. Chu, W. Zhu, N. Li, and L. E. Cross, J. Appl. Phys. **106** (2009).

[5] N. D. Sharma, R. Maranganti, and P. Sharma, J. Mech. Phys. Solids **55**, 2328 (2007).

[6] N. D. Sharma, C. M. Landis, and P. Sharma, J. Appl. Phys. **108**, 024304 (2010).

[7] H. Lu, C.-W. Bark, D. Esque De Los Ojos, J. Alcala, C. Eom, G. Catalan, and A. Gruverman, Science **335**, 59 (2012).

[8] E. V. Bursian and O. I. Zaikovskii, Sov. Phys. Solid State **10**, 1121 (1968).

[9] W. Ma and L. E. Cross, Appl. Phys. Lett. **88**, 232902 (2006).

[10] P. Zubko, G. Catalan, A. Buckley, P. R. L. Welche, and J. F. Scott, Phys. Rev. Lett. **99**, 167601 (2007).

[11] L. E. Cross, *J. Mater. Sci.*, J. Mater. Sci. **41**, 53 (2006).

[12] P. Hana, Ferroelectrics **351**, 196 (2007).

[13] W. Ma and L. E. Cross, Appl. Phys. Lett. **81**, 3440 (2002).

[14] J. Y. Fu, W. Zhu, N. Li, and L. E. Cross, J. Appl. Phys. **100**, 024112 (2006).

[15] J. Narvaez and G. Catalan, Appl. Phys. Lett. **104**, 162903 (2014).

[16] A. Klic and M. Marvan, Integ. Ferroelectrics **63**, 155 (2004).

[17] P. V. Yudin, R. Ahluwalia, and A. K. Tagantsev, Appl. Phys. Lett. **104**, 082913 (2014).

[18] P. Zubko, G. Catalan, and A. K. Tagantsev, Annu. Rev. Mater. Res. **43**, 387 (2013).

[19] A. Tagantsev and A. Yurkov, J. Appl. Phys. **112**, 044103 (2012).

[20] M. Stengel, Nature Commun. **4**, 2693 (2013).

[21] M. Stengel, Phys. Rev. B **90**, 201112 (2014).

[22] T. D. Nguyen, S. Mao, Y.-W. Yeh, P. K. Purohit, and M. C. McAlpine, Adv. Mater. **25**, 946 (2013).

[23] P. V. Yudin and A. K. Tagantsev, Nanotech. **24**, 432001 (2013).

[24] H. Le Quang and Q. C. He, Proc. Royal Soc. A **467**, 2369 (2011).

[25] L. Shu, X. Wei, T. Pang, X. Yao, and C. Wang, J. Appl. Phys. **110**, 104106 (2011).

[26] J. Hong and D. Vanderbilt, Phys. Rev. B **88**, 174107 (2013).

[27] M. C. Ray, J. Appl. Mech. **81**, 091002 (2014).

[28] S. Mao and P. K. Purohit, J. Appl. Mech. **81**, 081004 (2014).

[29] Z. Yan and L. Y. Jiang, J. Appl. Phys. **113**, 194102 (2013).

[30] M. S. Majdoub, P. Sharma, and T. Cagin, Phys. Rev. B **79** (2009).

[31] R. Ahluwalia, A. K. Tagantsev, P. Yudin, N. Setter, N. Ng, and D. J. Srolovitz, Phys. Rev. B **89**, 174105 (2014).

[32] Y. Gu, M. Li, A. N. Morozovska, Y. Wang, E. A. Eliseev, V. Gopala, and L.-Q. Chen, Phys. Rev. B **89**, 174111 (2014).

[33] H. Chen, A. Soh, and Y. Ni, Acta Mech. **225**, 1323 (2014).

[34] M. Arroyo and M. Ortiz, Int. J. Numer. Meth. Eng. **65**, 2167 (2006).

[35] A. Abdollahi, C. Peco, D. Millán, M. Arroyo, and I. Arias, J. Appl. Phys. **116**, 093502 (2014).

[36] R. Maranganti, N. D. Sharma, and P. Sharma, Phys. Rev. B **74**, 014110 (2006).

[37] A. E. Eliseev, A. N. Morozovska, M. D. Glinchuk, and R. Blinc, Phys. Rev. B **79**, 165433 (2009).

[38] N. D. Sharma, C. Landis, and P. Sharma, J. Appl. Phys. **111**, 059901 (2012).

[39] D. Millán, A. Rosolen, and M. Arroyo, Int. J. Numer. Meth. Eng. **85**, 723 (2011).

[40] W. Huang, X. Yan, S. R. Kwon, S. Zhang, F. G. Yuan, and X. Jiang, Appl. Phys. Lett. **101**, 252903 (2012).